Results in Physics 8 (2018) 578–583

Contents lists available at ScienceDirect

Results in Physics

journal homepage: www.journals.elsevier.com/results-in-physics

Neodymium cobalt oxide as a chemical sensor

I.A. Abdel-Latif [a,b,c,*], Mohammed M. Rahman [d], Sher Bahadar Khan [d]

[a] Department of Physics, Najran University, Najran, Saudi Arabia
[b] Reactor Physics Department, NRC, Atomic Energy Authority, Abou Zabaal, Cairo, Egypt
[c] Advanced Materials and Nano-Research Centre, Najran University, P.O. Box: 1988, Najran 11001, Saudi Arabia
[d] Chemistry Department, King Abdulaziz University, Faculty of Science, Jeddah 21589, P.O. Box 80203, Saudi Arabia

ARTICLE INFO

Article history:
Received 28 October 2017
Received in revised form 24 December 2017
Accepted 30 December 2017
Available online 3 January 2018

ABSTRACT

Chemical sensing and electrical transport properties of neodymium coblate, $NdCoO_3$, was investigated in this work. It was prepared by using co-precipitation method. Pure neodymium chloride and cobalt chloride were mixing in the presence of sodium hydroxide and the obtained co-precipitated powder was calcined at 850 and 1000 °C. The synthesized composites, as-grown ($NdCoO_3$-I), calcined at 850 °C ($NdCoO_3$-II), and calcined at 1000 °C ($NdCoO_3$-III) were studied in details in terms of their morphological and structural properties. The X-ray analysis confirmed that the synthesized products are well crystalline possessing single phase orthorhombic crystal system of space group *Pbnm* **(62)**. The crystallite size of $NdCoO_3$-I, $NdCoO_3$-II, and $NdCoO_3$-III is 22, 111, and 338 nm, respectively which reflect that crystallite size is increasing with increase in firing temperature. The DC resistivity was measured as a function of temperature in the temperature range from room temperature up to 200 °C. All $NdCoO_3$ are semiconductor in this range of temperature but showed different activation energy which strongly depends on the crystallite size of the products. The activation energy decreased with increase in crystallite size, 0.798, 0.414 and 0.371 eV for $NdCoO_3$-I, $NdCoO_3$-II, and $NdCoO_3$-III, respectively. Thus resistivity increases with increase in crystallite size of $NdCoO_3$. All $NdCoO_3$ products were tested as chemical sensor for acetone by electrochemical approaches and showed excellent sensitivity. Among the $NdCoO_3$ samples, $NdCoO_3$-III showed the highest sensitivity (3.4722 $\mu Acm^{-2}\,mM^{-1}$) compared to other compositions and gradually decreased to 3.2407 $\mu Acm^{-2}\,mM^{-1}$ with decreasing the crystallite size of $NdCoO_3$-II. It is also observed that the sensitivity drastically decreased to 0.76253 $\mu Acm^{-2}\,mM^{-1}$ in the case of $NdCoO_3$-I. It is introduced an efficient route for the detection of environmental unsafe chemicals by electrochemical approach for the safety of healthcare and environmental fields in broad scales.

Introduction

Monitoring the environment for hazardous chemicals is one of the important topics to save our environment clean and safe. So progress in materials for chemical and gas sensor detection took considerable scientific attention. In a chemical or gas sensor one can realize a change in electrical or optical output as a result of chemical and physical interactions with chemicals/gases. In particular, the chemical sensors [1–4] are useful in various safety applications where, we can determine any leakage. It is well known that perovskite oxides with ABO_3 formula were used as a gas sensor materials due to their stability in thermal and chemical atmospheres [5–7]. The deficient in oxygen in semiconducting oxide materials is responsible for the change in resistance of an oxide sensor due to the adsorbed surface species [5]. Nanostructured perovskite materials can improve the sensing properties of the sensor due to high surface-to-volume ratio characteristics. Knowledge of nanoscale perovskite sensing materials have been achieved a great attraction to serve as a novel gas sensing materials at the lower working temperatures. For high-temperature applications, perovskite oxides are very rich materials, where they have high melting and decomposition temperatures, furthermore they can provide microstructural and morphological stability to improve reliability and long-term sensor performance [8]. The $EuFe_{0.9}Co_{0.1}O_3$ oxides exhibit good gas sensing properties to acetone gas at the operating temperature of 280 °C [9]. According to Mekam et al., the hybridization between the transition metal cation and Oxygen atoms in the orthorhombic perovskites, is essential to weaken the short-range repulsion and allow the distortion. Besides, the rare earth cation can modify the ground state and nature of the transition by hybridizing with the valence state, that may indirectly cause change in the transition metal – oxygen

* Corresponding author at: Department of Physics, Najran University, Najran, Saudi Arabia.
E-mail address: ihab_abdellatif@yahoo.co.uk (I.A. Abdel-Latif).

https://doi.org/10.1016/j.rinp.2017.12.079
2211-3797/

interactions [10]. The electrical properties of any material are an important factor which help us to understand the transport phenomenon and related properties. To distinguish between the possible mechanisms, namely, band transfer, thermionic emission, thermally assisted tunneling and variable range hopping, the general behavior of the electrical resistivity must be determined. The DC electrical resistivity measurements as a function of temperature of $Eu_{0.65}Sr_{0.35}Mn_{0.7}Fe_{0.3}O_3$ and $Eu_{0.65}Sr_{0.35}Mn_{0.3}Fe_{0.7}O_3$ were reported in Refs. [11,12] this temperature dependence of the resistivity curve showed the semiconductor behavior where, resistivity decreases with increasing temperature. According to Parfenov et al., [13] electrical resistivity-temperature dependence of $Nd_{0.65}Sr_{0.35}Mn_{1-x}Fe_xO_3$ samples except $Nd_{0.65}Sr_{0.35}MnO_3$ manganite showed the activation temperature dependence of the specific resistance typical of semiconductors. Thermal conductivity of $NdCoO_3$ studied by Pillai [14] in the temperature range from 300 to 1200 K. The excitonic conductivity arising from the interactions of the t_{2g}–e_g states of cobalt ions in the oxides are showed with maxima at 1030 and 975 K, respectively, corresponding with their semiconductor-metal transition temperatures. Effect of Ni doping on the structural and electrical properties of $NdCoO_3$ was investigated by [15] where the conductivity measurements were carried out to investigate transport behavior of compounds. They found a drastic improvement of the room-temperature conductivity of $NdCo_{1-x}NixO_3$ (x = 0.1, 0.2) compared with the pure compound which explained in terms of decrease in band gap. By fitting Arrhenius and variable range hopping (VRH) models they explained behavior in different regions of temperature. The present work highlighted on the selective and sensitive chemical sensing and the electrical transport properties of neodymium coblate, $NdCoO_3$, and their correlation with crystal structure.

Experimental details

$NdCoO_3$ was prepared using co-precipitation method by dissolving the pure chlorides of neodymium, and cobalt in 100 mL distilled water then pure sodium hydroxide was added with the proper molar ratio. All together were stirred using magnetic stirring until we get the pH of our solution to be 12–13. The stirring process is maintained at 80 °C for 12 h then cooled down to the room temperature. Co-precipitated $NdCoO_3$ washed in distilled water until removing any powder of NaCl. The under investigation compounds in this work were fired at 850 °C and 1000 °C for 12 h. XRD measurements were performed with Cu radiation using a PANalytical X'pert Pro MPR diffractometer to check the formation of the required structure. The micrograph and elemental analysis measurements were carried out using Field Emission Scanning Electron Microscope FE-SEM – JEOL (JSM-5600) with acceleration voltage 15 kV and magnification of ×43,000. DC resistivity as a function of temperature was measured in the temperature range from room temperature up to 200 °C. Electrochemical I–V observation was executed at room condition by using the Keithley electrometer, where fabricated electrode and Pd-wire were used as working and counter electrode respectively.

Fabrication of senor

Silver electrode of surface area ~0.0216 cm^{-2} is coated with as-grown ($NdCoO_3$-I), calcined at 850 °C ($NdCoO_3$-II), and calcined at 1000 °C ($NdCoO_3$-III) using conducting binder such as butyl carbitol acetate and ethyl acetate (Fig. 1). All together are kept in the oven at 60 °C for 12 h until the film become completely uniform and dry. It is used as a working electrode and Pd wire is used as a counter electrode. Acetone is diluted in de-ionized water at different concentrations and used as a target analyte. Phosphate

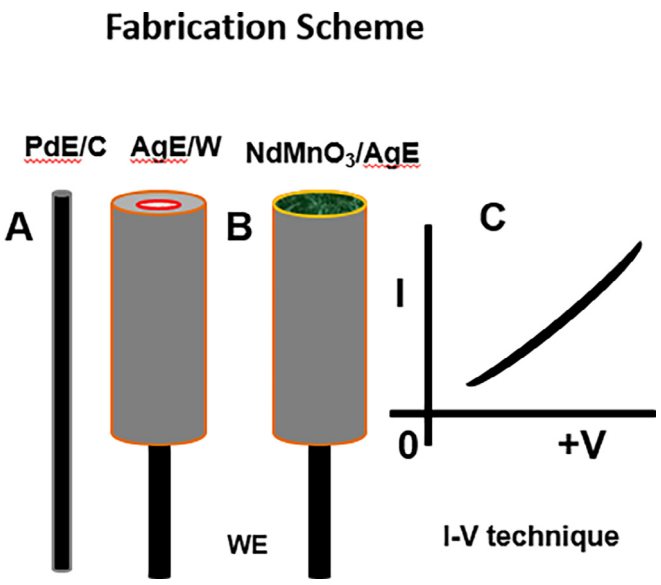

Fig. 1. 257175914400 Fabrication scheme of $NdCoO_3$ coated AgE for chemical sensor development.

buffer solution (PBS, 0.1 M, pH 7.0) is prepared by mixing 0.2 mol of Na_2HPO_4 and 0.2 mol of NaH_2PO_4 solutions in 100.0 mL of de-ionized water. Amount of 0.1 M PBS was kept constant as 10.0 mL for all measurement. The pH of the solution is kept constant because increase in pH affects the efficiency of the electrochemical experiment which may be due increase in ion carriers. PBS was used for total investigations of chemical sensor development and its performance. The different samples of $NdCoO_3$ coated electrode has been primarily investigated in absence of Acetone by I–V technique. After injecting the acetone drop-wise (100.0 μL) into bulk solution, the similar technique is used to measure the conducting current against applied voltage. The ratio of voltage and current (slope) is calculated as a measure of acetone sensitivity.

Results and discussions

XRD diffraction patterns of $NdCoO_3$ as prepared and annealed at 850 °C and 1000 °C are shown in Fig. 2a. Sample $NdCoO_3$ I (as grown) is not completely formed but after firing at 850 °C for $NdCoO_3$ II and 1000 °C for $NdCoO_3$ III samples it is clear that both samples are completely crystalline and both patterns are refined using Fullprof program [16], see Fig. 2b. It is quite clear that all reflections belong to the orthorhombic crystal system of *Pbnm* space group (No. 62) where the maximum refection intensity at 112 planes is observed and no other phases are exist. The lattice parameters are listed in Table 1. The Nd atoms occupy (x, 1/4, z) position while Co atoms occupy (0, 0, 1/2) position and surrounded by octahedral oxygen atoms. The oxygen atoms in this compound are distributed as following; four of them occupy the (x, 1/4, z) position and eight have (x, y, z) position. The bond lengths between Co—O and Co—O—Co angles were calculated and they are listed in Table 1.

There are slightly differences in the positions of Nd-Co-O atoms in $NdCoO_3$-II, and $NdCoO_3$-III, which still possess the same phases. This difference leads to change in distortion. Jahn-Teller distortion is given by the octahedral distortion parameter Δd which defined as [17].

$$\Delta d = \frac{1}{6}\sum_{n=1}^{6}\left[\frac{(dn-d)}{d}\right]^2$$

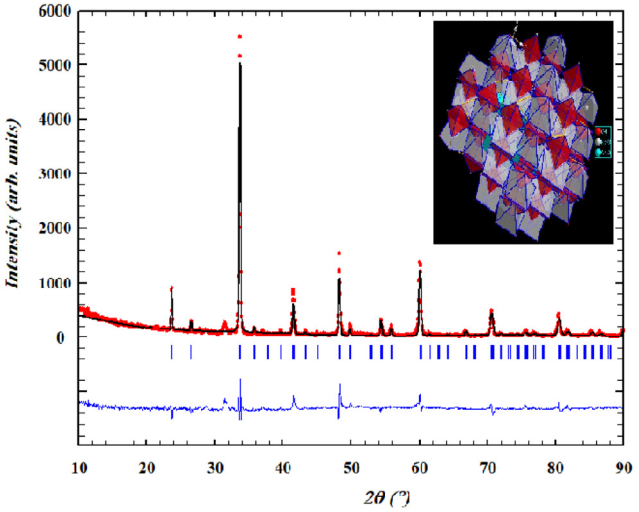

(b)

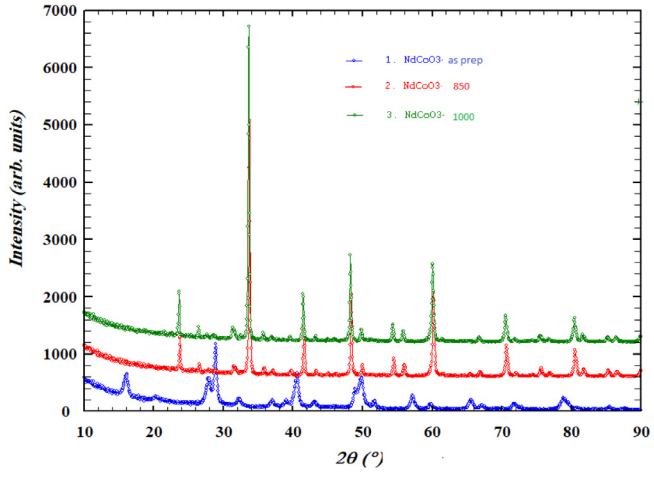

(a)

Fig. 2. (a) XRD patterns of $NdCo_3$ I, $NdCo_3$ II, and $NdCo_3$ III (b) XRD diffraction pattern of $NdCo_3$ III, Rietveld refinement and the difference.

where d is the mean cobalt-oxygen bond distance (Co—O) and d_n are the individual cobalt-oxygen (Co—O) bond distances. The calculated distortion for $NdCoO_3$-II, and $NdCoO_3$-III showed that there slight difference in distortion of the orthorhombic unit cells; ($\Delta d \sim 1.26 \times 10^{-1}$ and $\Delta d \sim 1.34 \times 10^{-1}$). To evaluate the effect of annealing on the lattice distortion we applied the following formula [18];

$$D = \frac{1}{3}\sum_{i=1}^{3} 10^{-4} \times \left| \frac{(a_i - \overline{a})^2}{\overline{a}^2} \right|$$

where

$a_1 = a/\sqrt{2}$, $a_2 = /b\sqrt{2}$, $a_2 = b$, $a_3 = c/\sqrt{2}$, and $\overline{a} = \frac{a_1+a_2+a_3}{3}$

We found lattice distortion values to be D = (2.91×10^{-6} and 2.92×10^{-6}) to confirm that both samples have the same distortion.

The crystalline size δ as a result of annealing is calculated using the well-known Scherrer formula; [19]

$$\delta = k\lambda/(\mathrm{B}\sin\theta)$$

where B is FWHM and equal to $B_{obs.} - B_{std.}$ ($B_{obs.}$ is FWHM of observed sample and B_{std} is FWHM of standard sample). The crystalline size of $NdCoO_3$ are listed in Table 1. The crystallite size of $NdCoO_3$-I, $NdCoO_3$-II, and $NdCoO_3$-III is 22, 111, and 338 nm, respectively which reflect that crystallite size is increasing with increase in firing temperature.

The microstructure graph of $NdCoO_3$ II is illustrated in Fig. 3. It is quite clear that there is homogeneity in the crystalline size all over the graph. The mean value of the particle size of $NdCoO_3$ is 160 nm, deduced from SEM graphs, compared with the crystalline size deduced from XRD measurements (111 nm) which showing the good agreement. Overall we found good agreement in the deduced values of particle size deduced from both the SEM micrograph and the XRD diffraction. The energy dispersive spectroscopy EDS reveals that the synthesized composite is obtained in proper stoichiometry of the proposed structure. So one can conclude, from the elemental analysis, that all synthesized samples formed according to the proposed elements in composites are well formed with the proper stoichiometry.

The variation in DC resistivity as a function of temperature was measured in the temperature range from room temperature up to 200 °C, see Fig. 4. The resistivity increase with increasing temperature for all $NdCoO_3$ which in an indication to the semiconductor behavior in this range of temperature but with different activation energy which strongly depends on the crystallite size of the products. This behavior is similar to those reported before in Refs. [11–15]. The activation energy decreased with increase in crystallite size, 0.798, 0.414 and 0.371 eV for $NdCoO_3$-I, $NdCoO_3$-II, and $NdCoO_3$-III, respectively. Thus resistivity increases with decrease in crystallite size of $NdCoO_3$.

Chemical sensing investigations

All $NdCoO_3$ products were tested as chemical sensor for acetone and showed the higher sensitivity. Fig. 5 show an I–V diagram of $NdCoO_3$-I, $NdCoO_3$-II, and $NdCoO_3$-III, after exposure to the acetone. The electrical response of conventional silver electrode (dark-dotted) and $NdCoO_3$ coated silver electrode (gray-dotted) are shown in Fig. 5(a). Fig. 5(b) show electrical responses of the $NdCoO_3$ without acetone (gray-dotted line) and with 100.0 μL acetone (dark-dotted line). It is observed that by injecting the acetone, $NdCoO_3$ samples show a significant increase in the electrical current which reflects the sensing of $NdCoO_3$ to acetone Fig. 6.

The fast electron exchange and good electro-catalytic oxidation properties are responsible for the high electrical response of various $NdCoO_3$ fabricated AgE sensor to acetone [20,21]. Acetone easily undergoes catalytic dissociation reaction by applying to I–V technique. The catalytic reaction of acetone produces $2H^+$ and $2e^-$ (increase the carrier ions) which increases the conductivity of the host $NdCoO_3$ material by providing excess electron to the conduction band of the material. According to the microscopic model reported earlier [22–24] that subsequent emission of an

Table 1
Lattice parameter of $NdCoO_3$ at different annealing temperature.

	a, Å	*b*, Å	*c*, Å	Cell Vol., Å^3	Cryst. Size, nm	<Co-O> Å	Co-O-Co
$NdCoO_3$-II	5.3268	5.3133	7.5143	212.676	111	2.56	169.8
$NdCoO_3$-III	5.3413	5.3211	7.5243	213.854	338	2.47	165.34

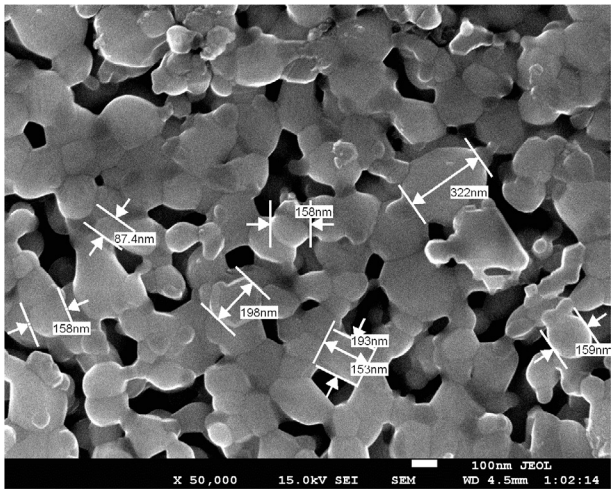

Fig. 3. Morphological evaluation by FESEM for $NdCo_3$ II.

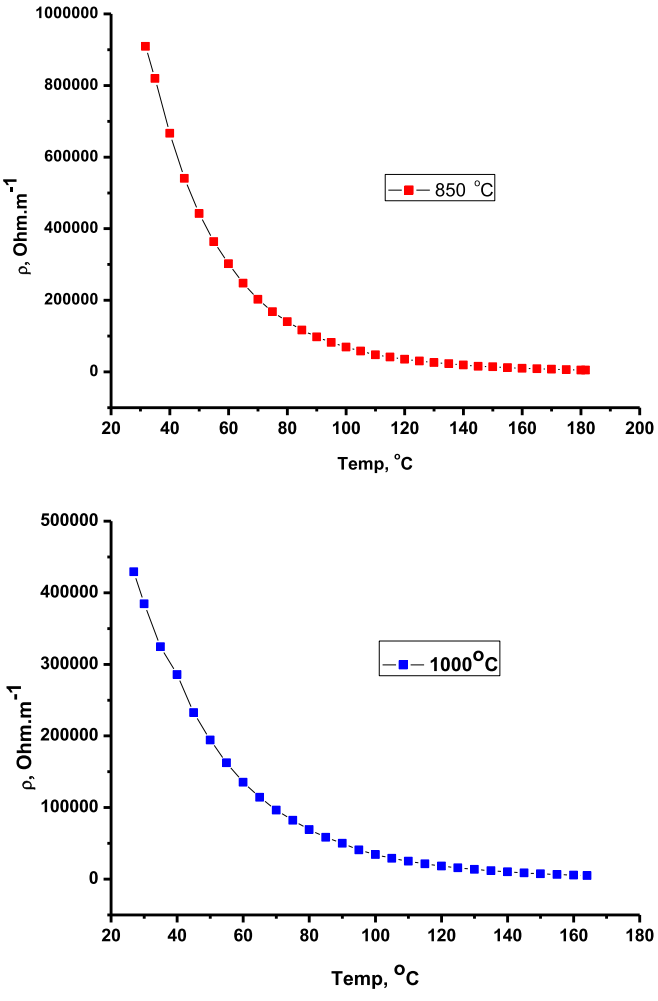

Fig. 4. The variation of resistivity of $NdCo_3$ II and $NdCo_3$ as a function of temperature.

electron take place from the chemisorbed oxygen species into the conduction band of the sensor and cause change in the electrical conductance of the sensor due to the two reactions. In the first reaction atmospheric oxygen molecules are physisorbed on the surface sites, which while moving from site to site, get ionized by extracting an electron from the conduction band and are thus ionosorbed on the surface as O^-_{ads} (O— or O^-_2 depending on the energy available).

The effect of acetone concentration [6.7 M–0.13 mM] on the I–V response of $NdCoO_3$ sensors have been investigated (Fig. 5c). It is observed that with increasing acetone concentration, the current was gradually increased. This is explained by the conductivity of $NdCoO_3$ sensors increased which is ascribed to the increase in ions providing excess electron to the conduction band of the sensors [20,21,25,26]. Calibration curve of the $NdCoO_3$ sensor which is plotted from the variation of acetone concentration is shown in Fig. 5(d). Initially response current increases as the concentration of acetone increases and after certain concentration electrical response become constant and thus saturation takes place at high concentration above 0.13 M. Calibration curve depicts two sensitivity regions; at lower concentrations is linear up to 0.13 mM and 0.13 M for $NdCoO_3$ with correlation coefficient (R) of 0.9413. The sensitivity is calculated from the slope of the lower concentration region of calibration curves, which is 0.76253 $\mu A.cm^{-2}.mM^{-1}$ (As-grown sample), 1.2860 $\mu A.cm^{-2}.mM^{-1}$ (for calcined at 850 °C), and 1.4188 $\mu A.cm^{-2}.mM^{-1}$ (for calcined at 1000 °C) for all $NdCoO_3$ respectively. The first region appears to be the most sensitive region for acetone detection. The saturation region at higher concentration might be due to the unavailability of free $NdCoO_3$ sites for acetone adsorption. The linear dynamic range of this sensor exhibits from 0.13 mM to 0.13 M and the detection limit was estimated, based on signal to noise ratio (S/N), to be 18.0 μM. Above 0.13 M acetone for $NdCoO_3$ sensors become saturated either porosity and particle like shapes. This is explained by the sensitivity of calcined $NdCoO_3$ (at 1000 °C) particles is higher than as grown sample. We mentioned in the previous sections so the conductivity of calcined $NdCoO_3$ is higher than as-grown $NdCoO_3$ and this led to increase in ions providing excess electron to the conduction band of the $NdCoO_3$/AgE sensors [20–21,25–26]. The behavior of calcined $NdCoO_3$ based aqueous acetone sensor was compared with the previously reported sensors. Calcined $NdCoO_3$ showed significantly higher sensitivity and lower detection limit than those of previously reported acetone sensors [23,27,28]. The sensitivity obtained for the present calcined $NdCoO_3$ is much faster than those obtained for other materials [22,28], which is possibly due to the effective diffusion at the calcined $NdCoO_3$ surface. We carried experimental work within 6–8 weeks, through this period we observed that the materials are stable during storage under normal conditions. Therefore, one can conclude that $NdCoO_3$ are good candidate, compared to other materials for the fabrication of efficient and highly sensitive chemical sensor.

Conclusion

Finally, we have successfully fabricated acetone chemical sensor based on various $NdCoO_3$ materials, which is immobilized onto side-polished AgE with conducting binders for the first time. $NdCoO_3$ materials are prepared by by using co-precipitation method, which represents a simple and economical approach. Analytical performances of acetone chemical sensor are investigated by reliable I-V method in terms of sensitivity, linearity, and detection limit in short response time. This extensive research is performed in terms of preparation and characterization of calcined $NdCoO_3$ nanomaterials and applied for the acetone sensor using I–V method. Hence, this approach is introduced a new route for efficient chemical sensor development in environmental and healthcare fields.

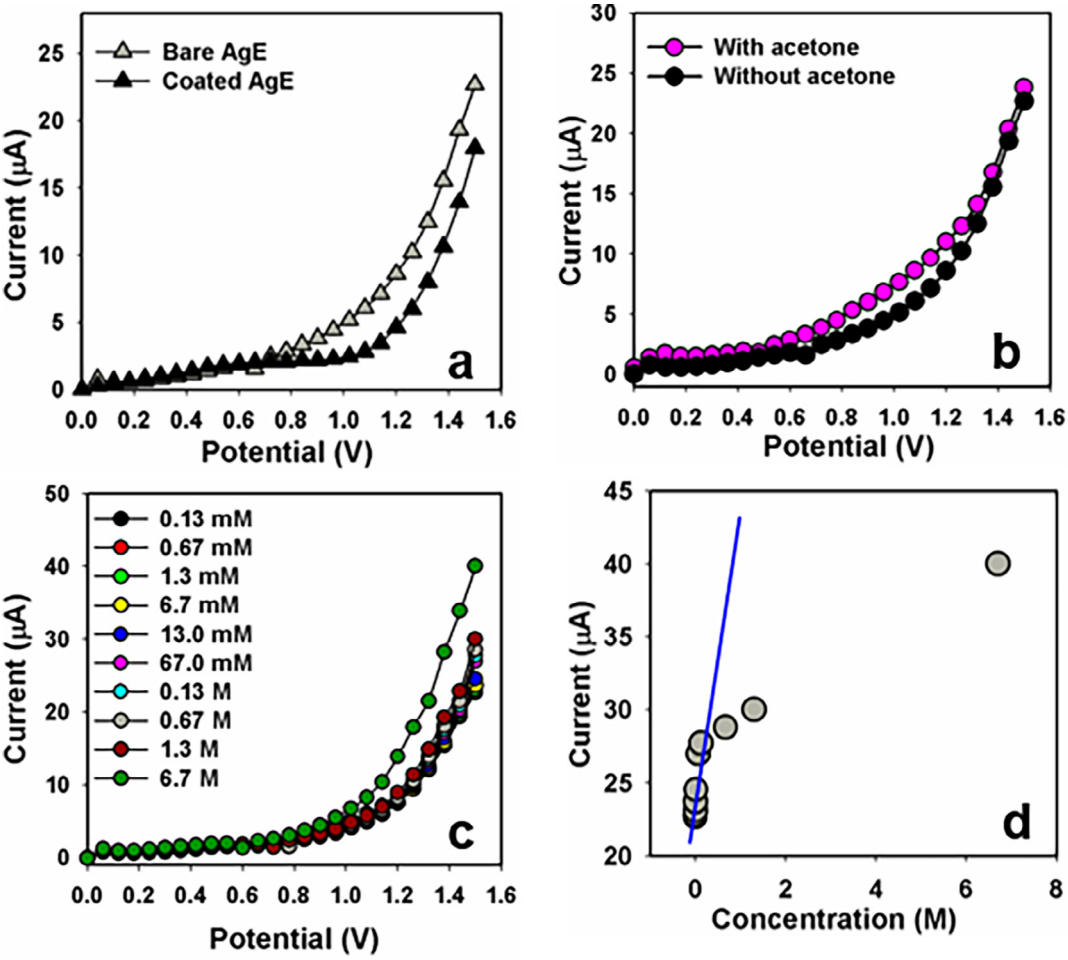

Fig. 5. I–V characteristic as a result of acetone. (a) control experiment, (b) Without and with acetone, (c) concentration variation curve, and (d) calibration curve.

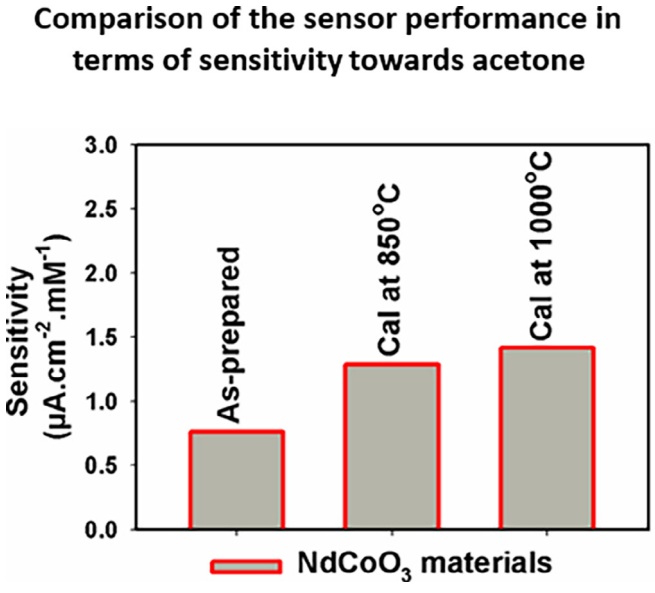

Fig. 6. Comparative performance of acetone sensitivity of all $NdCoO_3$ coated AgE.

Acknowledgements

Najran University is acknowledged for financial support during the course of this work. Center of Excellence for Advanced Materials (CEAMR) and Chemistry Department, King Abdulaziz University, Jeddah is highly acknowledged.

References

[1] M Enhessari and A Salehabadi, Chapter from Progresses in Chemical Sensor book (2016), pp. 60–91: https://doi.org/10.5772/62559.
[2] Khan SB et al. New J Chem 2013;37:1098.
[3] Riegel J, Neumann H, Wiedenmann H-M. Solid State Ionics 2002;152–153:783.
[4] Wang X, Qin H, Sun L, Hu J. Sensors Actuators B Chem 2013;188:965–71.
[5] Zhou Z-G et al. Sensor Actuator B 2001;77:22.
[6] Arakawa T., Perovskites as solid state chemical sensors in: LG Tejuca, JL Ferro Ed. Marcel Dekker, New York, 1993, Ch 19 pp 361- 1995 79-86.
[7] Ling T-R, Chen ZB, Lee MD. Catalysis Today 1995;26:79.
[8] Fergus JW. Sensors Actuators B. 2007;123:1169–79.
[9] Kan H, Zhao Y, Liu Y, Li Y, Zhao H. Adv Mater Process 2010:271–4. https://doi.org/10.1142/9789814322799_0063.
[10] Mekam M et al. Results Phys 2012;2:156–63.
[11] Parfenov VV et al. Russian Phys J 2003;46:979.
[12] Abdel-Latif IA. IOP Conf Series Mater Sci Eng 2016;146:012003. https://doi.org/10.1088/1757-899X/146/1/012003.
[13] Abdel-Latif IA, Saleh SA. J Alloys Comp 2012;530:116–20.
[14] Pillai CGS, George AM. Int J Thermophys 1991;12:207–21.
[15] V. Kumar et al. AIP Conf Proc 1447 2012 975 https://doi.org/10.1063/1.4710330.
[16] Rodriguez-Carvajal. J. Physica B 1993;192:55.
[17] Abdel-Latif IA et al. J Taiwan Inst Chem Eng 2017;75:174.
[18] Ardit M., Dondi M., Cruciani G. Chapter in book: Minerals as Advanced Materials II: Lattice Distortion Upon Compression in Orthorhombic Perovskites: Review and Development of a Predictive Tool, Publisher: Springer, Editors: Sergey V. Krivovichev, 2012: pp. 305–318 (DOI: 10.1007/978-3-642-20018-2_29).
[19] Abdel-Latif IA, Ismail AA, Bouzid H, Al-Hajry A. J Magn Magn Mater 2015;393:233–8.
[20] Song M-J, Hwang SW, Whang D. Talanta 2010;80:1648–52.

[21] Yuan C, Xu Y, Deng Y, Jiang N, He N, Dai L. Nanotechnology 2010;21:415501.
[22] Rahman MM, Jamal A, Khan SB, Faisal M. ACS Appl Mater Interfaces 2011;3:1346–51.
[23] Rahman MM, Jamal A, Khan SB, Faisal, Asiri AM. Sens. Transducers J. 2011;134:32–44.
[24] Langford J, Lover D. J. Appl. Crystallogr. 1991;24:149.
[25] Teng F, Yao V, Zheng Y, Ma Y, Teng Y, Xu T, Liang S, Zhu Y. Sens Actuators B 2008;134:761–8.
[26] Akhavan O, Ghaderia EJ. Mater Chem 2011;21:12935.
[27] El-Safty SA, Ismail AA, Matsunaga H, Hanaoka T, Mizukami F. Adv Funct Mater 2008;18:1485–500.
[28] Chitravathi S, Swamy BEK, Chandra U, Mamatha GP, Sherigara BS. J Electroanal Chem 2010;645:10–5.